Transcriptional pattern enriched for synaptic signaling is associated with shorter survival of patients with high-grade serous ovarian cancer

Arkajyoti Bhattacharya [#,1],PhD, Thijs S. Stutvoet [#,1],MD, PhD, Mirela Perla[#,1],MSc, Stefan Loipfinger[1], MSc, Mathilde Jalving[1],MD, PhD, Anna K.L. Reyners[1],MD, PhD, Paola D. Vermeer[2], PhD, Ronny Drapkin[3],MD, PhD, Marco de Bruyn[4],PhD, Elisabeth G.E. de Vries[1],MD, PhD, Steven de Jong[1],PhD, Rudolf S.N. Fehrmann [*,1],MD, PhD

[1]Department of Medical Oncology, University Medical Center Groningen, University of Groningen, Groningen, the Netherlands, [2]Cancer Biology and Immunotherapies Group, Sanford Research, Sioux Falls, SD, [3]Penn Ovarian Cancer Research Center and Basser Center for BRCA, University of Pennsylvania, Perelman School of Medicine, Philadelphia, PA, [4]Department of Obstetrics and Gynecology, University Medical Center Groningen, University of Groningen, Groningen, the Netherlands

[#] Contributed equally

[*]**Corresponding author:**

Rudolf S.N. Fehrmann, MD, PhD

Department of Medical Oncology, University Medical Center Groningen

P.O. Box 30.001, 9700 RB Groningen, the Netherlands

Tel. +31503612821, Fax +31503614862

E-mail: r.s.n.fehrmann@umcg.nl

Abstract

Background: Bulk transcriptomic analyses of high-grade serous ovarian cancer (HGSOC) so far have not uncovered potential drug targets, possibly because subtle, disease-relevant transcriptional patterns are overshadowed by dominant, non-relevant ones. Our aim was to uncover disease-outcome-related patterns in HGSOC transcriptomes that may reveal novel drug targets.

Method: Using consensus-independent component analysis, we dissected 678 HGSOC transcriptomes of systemic therapy naïve patients—sourced from public repositories—into statistically independent transcriptional components (TCs). To enhance c-ICA's robustness, we added 447 transcriptomes from non-serous histotypes, low-grade serous, and non-cancerous ovarian tissues. Cox regression and survival tree analysis were performed to determine the association between TC activity and overall survival (OS). Finally, we determined the activity of the OS-associated TCs in 11 publicly available spatially resolved ovarian cancer transcriptomes.

Results: We identified 374 TCs, capturing prominent and subtle transcriptional patterns linked to specific biological processes. Six TCs, age, and tumor stage stratified patients with HGSOC receiving platinum-based chemotherapy into ten distinct OS groups. Three TCs were linked to copy-number alterations affecting expression levels of genes involved in replication, apoptosis, proliferation, immune activity, and replication stress. Notably, the TC identifying patients with the shortest OS captured a novel transcriptional pattern linked to synaptic signaling, which was active in tumor regions within all spatially resolved transcriptomes.

Conclusion: The association between a synaptic signaling-related TC and OS supports the emerging role of neurons and their axons as cancer hallmark-inducing constituents of the tumor microenvironment. These constituents might offer a novel drug target for patients with HGSOC.

Keywords: high-grade serous ovarian cancer (HGSOC), synaptic signaling, consensus independent component analysis, transcriptome

Background

Epithelial ovarian cancer encompasses five primary histological subtypes, with high-grade serous ovarian carcinoma (HGSOC) constituting about 75% of all cases (1). The standard treatment for HGSOC diagnosed at stage IIB and beyond involves a combination of surgery and chemotherapy, primarily using platinum-based compounds and taxanes (2,3). While initial chemotherapy results in tumor response in most patients with HGSOC, there is a very high recurrence rate (4). The addition of poly-ADP ribose polymerase and vascular endothelial growth factor A inhibitors to chemotherapy for subsets of patients currently results in a 5-year disease-specific overall survival (OS) rate of approximately 45% for patients with HGSOC. This rate has hardly improved in the last three decades (5–8). Therefore, new insights into the complex biology underlying HGSOC are urgently needed to develop more effective treatment strategies.

Previous studies using bulk transcriptomes of patients with HGSOC have identified expression-based molecular subtypes. However, these subtypes did not provide insights that have translated into novel drug targets (9–11). A common limitation of such studies is their reliance on bulk transcriptomes, containing both tumor cells and tumor microenvironment (TME) components, thus reflecting the average transcriptional patterns of the combination of all biological processes present in the tumors. This averaging often masks subtle transcriptional patterns pivotal to understanding HGSOC biology, especially when these are overshadowed by dominant patterns from other less relevant (non-)biological processes (12). Consensus-independent component analysis (c-ICA) offers an alternative by decomposing such bulk transcriptomes into statistically independent transcriptional patterns (i.e., transcriptional components; TCs)(13,14). This approach reveals both dominant and subtle patterns and provides a measure of TC activity for each sample (15).

74 In the present study, our aim was to utilize c-ICA to dissect HGSOC transcriptomes to identify
75 as many TCs associated with patient OS as possible, which could reveal potential novel drug
76 targets.

77 Methods

78 See Supplementary methods for the extended methods.

79 **Data acquisition**

80 Raw microarray bulk transcriptomes and clinicopathological details for patients with HGSOC,
81 low-grade serous ovarian cancer (LGSOC), non-serous ovarian cancer, and benign ovarian
82 tissues were sourced from the Gene Expression Omnibus (GEO)(16). We exclusively utilized
83 transcriptomes generated from primary tumor samples. Our analysis was confined to
84 samples on the Affymetrix HG-U133 Plus 2.0 platform (GEO accession identifier: GPL570)
85 and excluded cell line samples. The datasets were pre-processed, and quality controlled as
86 previously described (17). Furthermore, for comprehensive analyses, we incorporated
87 transcriptomes from five distinct resources: the Cancer Cell Line Encyclopedia (CCLE, n =
88 969), Genomics of Drug Sensitivity in Cancer (GDSC, n = 959), Gene Expression Omnibus
89 (GEO, n = 13,810), and The Cancer Genome Atlas (TCGA, n = 8,150), and spatially resolved
90 transcriptomes from 10xGenomics (16,18-20).

91

92 **Consensus-independent component analysis (c-ICA)**

93 The bulk transcriptome input data underwent a whitening transformation to optimize the
94 subsequent analysis. Following this pre-processing step, we employed the FastICA algorithm
95 to execute the ICA, facilitating the derivation of estimated sources (ESs). We determined the
96 appropriate number of ESs to extract based on the number of principal components that

97 captured 90% of the total variance within the dataset. To rigorously evaluate the stability of
98 the ESs, we conducted 25 separate ICA runs, each with uniquely randomized initial weight
99 factors. ESs with an absolute Pearson correlation exceeding 0.9 were grouped. By analyzing
100 the outcome of these runs, we derived consensus ESs, denoted as transcriptional
101 components or TCs. This was achieved by computing the mean vector of weights from
102 grouped ESs present in over half of the conducted runs. The gene weights within each TC
103 provide insights into the strength and directionality by which an underlying latent biological
104 process influences the related gene expression levels. Subsequently, these TCs are used to
105 generate a consensus mixing matrix (MM). The coefficients within this MM depict the
106 activity scores of the TCs across the samples.
107
108 **Survival analysis**
109 To discern the relationship between TC activity and patient OS, a univariate Cox proportional
110 hazards analysis was conducted on a select group of patients with available follow-up data (*n*
111 = 541, Supplementary Table S1). In addition, a multivariate Cox proportional hazards analysis
112 was carried out, including covariates such as age, stage, debulking status, and tumor grade.
113 This latter analysis was based on a subset of patients with comprehensive clinicopathological
114 data available (*n* = 373, Supplementary Table S1). We implemented a multivariate
115 permutation framework encompassing 10,000 permutations to mitigate the risk of false
116 discoveries. We established the acceptable false discovery rate (FDR) at 1%, maintaining an
117 80% confidence level, applicable for both the univariate and multivariate analyses.
118
119 **Survival tree analysis**

120 We performed a survival tree analysis to delineate groups of patients with HGSOC treated
121 with platinum-based chemotherapy based on distinct transcriptional and clinicopathological
122 attributes. The analysis utilized activities of TCs associated with OS (either from univariate or
123 multivariate survival analysis as mentioned in supplementary methods) in conjunction with
124 relevant clinicopathological factors, such as age, tumor stage, debulking status, and grade, as
125 potential classifiers. We divided patients into two subsets using every plausible cut-off point
126 for each classifier and compared the resulting survival curves employing the log-rank
127 statistic. Consequently, the division was based on the most significant classifier at its optimal
128 cut-off based on the smallest p-value of the log-rank test mentioned above. This divisional
129 process was successfully reiterated on the derived subsets until any of the following
130 stipulated conditions was satisfied: *i*) the total patient count across both subsets fell below
131 50, *ii*) the collective number of uncensored events in both subsets was < 25, or *iii*) one of the
132 subsets contained < 17 patients. To gauge the stability of our classifiers, we performed
133 20,000 iterations, randomly selecting 80% of the patient group in each iteration. The
134 significance-based ranks of classifiers in these iterations were correlated with those from the
135 primary survival tree.
136

137 **Associating the identified transcriptional components with biological processes**

138 To discern the biological processes associated with the TCs, we adopted a multifaceted
139 approach encompassing *i*) Transcriptional Adaptation to Copy Number Alterations (TACNA)
140 profiling, targeting the identification of TCs that reflect the downstream implications of copy
141 number alterations (CNAs) on gene expression levels(21); *ii*) Execution of gene set
142 enrichment analysis (GSEA) for each TC, utilizing gene set collections (n = 16) from The
143 Human Phenotype Ontology (The Monarch Initiative), the Mammalian Phenotypes (Mouse

144 Genome Database), and the Molecular Signatures Database (MsigDB)(22,23); *iii*) The
145 formation of co-functionality networks on the top and bottom genes of each TC, achieved
146 using the GenetICA methodology, accessible via https://www.genetica-network.com(24). For
147 clusters comprising ≥ 5 genes, the enrichment of the predicted functionality was quantified.
148 This served as the foundation for determining the biological process associated with the TC
149 being examined.
150
151 **Cross-study transcriptional component projection**
152 To determine whether a biological process captured by an identified TC is also active in other
153 cancer types and to investigate if it is more active in tumor cells or in the TME, we collected
154 raw expression profiles from multiple sources: the Cancer Cell Line Encyclopedia (CCLE, n =
155 969), Genomics of Drug Sensitivity in Cancer (GDSC, n = 959), Gene Expression Omnibus
156 (GEO, n = 13,810), and The Cancer Genome Atlas (TCGA, n = 8,150)(16,22–24). While the
157 CCLE and GDSC datasets comprise cell line profiles across many solid and hematologic
158 malignancies, the GEO and TCGA datasets offer an extensive set of bulk transcriptomes
159 derived from patient samples spanning 27 tumor types. We pre-processed the raw data as
160 previously described (18). Next, we projected the TCs identified via c-ICA onto the cell line
161 expression profiles from CCLE and GDSC and the patient-derived expression profiles from
162 GEO and TCGA. This projection methodology has been described in more detail previously
163 (18). To identify potential variations in the activity scores of the TCs, we compared the
164 activity scores among cell lines and samples derived from patients within all four
165 repositories. We used an absolute activity score threshold of 0.05 for each TC to pinpoint
166 outlier cell lines and patient tumors with heightened activity.
167

168 **Determination of spatial transcriptomic profiles' significant activity locations for individual**
169 **transcriptional components**

170 To further assess whether a biological process captured by an identified TC is more active in
171 tumor cells or in the TME, we collected publicly available spatial resolved transcriptomic
172 profiles of ovarian cancer samples. Eight were sourced from GEO (study ID GSE211956), and
173 three were sourced from the public dataset repository of 10xGenomics (see supplementary
174 methods for details) generated using the 10xGenomics Visium platform. The samples were
175 from patients with HGSOC, serous papillary, and endometrioid ovarian cancer. Activity for
176 each TC across every location within the spatial samples was ascertained through the cross-
177 study projection methodology referred to in the previous method section (21). We
178 incorporated a permutation-driven approach to discern the markedly active areas within the
179 spatial samples for each TC. We derived a null distribution of activities for each TC-location
180 pairing by performing 3,000 permutations and subsequent projections. The p-value of each
181 observed TC activity quantifies the significance of the deviation of the TC activity at a given
182 location from its baseline null distribution. After this, we visualized the z-transformed p-
183 values using a heatmap, followed by obtaining colocalization scores for each combination of
184 TCs in the spatial transcriptomic profiles for each ovarian cancer sample (25). This
185 visualization aided in highlighting the areas with notable activity aligned against the stained
186 representation of the tissue sample.

187

188 ## Results

189 **An integrated data set containing 1,125 bulk transcriptomes from ovarian tissues**

190 We curated 1,193 bulk transcriptomes from the GEO, including patients with HGSOC, low-
191 grade serous ovarian cancer (LGSOC), non-serous ovarian cancer, and benign ovarian tissues

192 (16). Pre-processing, which included removing duplicates and quality checks, culminated in a
193 refined dataset of 1,125 samples (17). These were extracted from 32 distinct studies
194 (Supplementary Table S2) and represented the entire spectrum of ovarian cancer types,
195 stages, and grades, and included 43 samples from non-malignant ovarian tissue
196 (Supplementary Table S1). The ovarian cancer dataset comprised bulk transcriptomes of
197 patients with HGSOC (*n* = 678), other serous (*n* = 110), endometrioid (*n* = 110), and clear-cell
198 ovarian cancer samples (*n* = 96). Additionally, for 541 patients, comprehensive survival data
199 was available, as well as additional clinicopathologic information, including age, grade, stage,
200 subtype, treatment schedule, and debulking status for 373 patients (Fig. 1).
201
202 **Consensus-independent component analysis identifies 374 transcriptional components**
203 c-ICA on the 1,125 bulk transcriptomes revealed 374 independent TCs. Notably, 135 TCs
204 captured the impact of copy number alterations on gene expression levels. Each TC
205 displayed enrichment for at least one gene set from the 16 gene set collections, with an
206 absolute Z-score of more than two. For example, the number of enriched gene sets from the
207 Hallmark gene set collection in an individual TC ranged from zero to 28 enriched gene sets
208 (interquartile range 3 – 7). The median top Z score for Hallmark gene sets was 3.21 (range
209 1.55 – 37.54, interquartile range 2.6 – 4.25). A comprehensive database, including all TCs
210 and GSEA outcomes, has been made accessible at http://transcriptional-landscape-
211 ovarian.opendatainscience.net.
212
213 Using consensus-independent component analysis (c-ICA), we decomposed the 1,125 bulk
214 transcriptomes, revealing 374 independent transcriptional components (TCs). Each TC
215 displayed enrichment for at least one gene set from the 16 gene set collections, with an

216 absolute Z-score of more than two. The activities of 13 TCs were associated with patient
217 overall survival (OS) in a univariate analysis, with an additional TC (TC166) identified in a
218 multivariate analysis accounting for age, stage, debulking, and tumor grade. Combined,
219 these 14 OS-associated TCs were enriched for gene sets associated with diverse biological
220 processes and clinicopathological characteristics, with four TCs capturing the effects of copy
221 number alterations on gene expression levels.
222
223 **The activities of six transcriptional components are associated with patient overall survival**
224 For a selected subset of 541 patients—including HGSOC, LGSOC, and non-serous ovarian
225 cancer—with available OS information (Supplementary Table S1), 13 TC activities displayed
226 an association with OS univariately (false discovery rate 5%, confidence level 80% in
227 permutation-based multiple testing framework Supplementary Table S3; Fig. 2). For patients
228 with serous ovarian cancer, treated with platinum-based therapy (n = 301, Supplementary
229 Table S1), lower activity of one additional TC (TC166) was associated with worse OS
230 independent of age, stage, debulking, and tumor grade (Supplementary Table S4).
231 Combined, these 14 OS-associated TCs were enriched for gene sets associated with diverse
232 biological processes and clinicopathological characteristics. Four of these TCs captured the
233 downstream effects of CNAs on gene expression levels (Fig. 2, Supplementary Fig. S1-S3).
234 Survival tree analysis identified ten groups of patients with platinum-treated HGSOC based
235 on the activity of six OS-associated TCs and the presence of two clinicopathological
236 characteristics, namely age and stage (Fig. 3, Supplementary Table S5, median robustness
237 statistic of survival tree = 0.52, interquartile range = 0.36 - 0.69). The survival tree
238 demonstrated good classification power (concordance statistic = 0.72, standard error =
239 0.021). As expected, patients were divided into separate survival groups based on stage (1/2

240 vs. 3/4) and age (<53.7 vs. ≥53.7 years). The most significant difference in OS was observed
241 between the cohorts with low and high TC121 activity (Supplementary Table S5). Patients
242 with high TC121 tumor activity exhibited the shortest OS, also observed for the subset of
243 patients with advanced-stage HGSOC (Supplementary Fig. S4, Supplementary Table S6).
244 These robust associations with OS for TC121 in these two subsets of patients indicate the
245 relevance of TC121, irrespective of stage.
246
247 **Distinct biological processes show enrichment in the transcriptional components**
248 **associated with overall survival**
249 Three of the six TCs associated with OS—TC166, TC247, and TC76—captured the effects of
250 CNAs on the expression levels of genes mapping to chromosome regions 13q12-q14, 11q13-
251 q14, and 9p13-p21, respectively (Supplementary Fig. S5, Supplementary Table S7) (6). The
252 higher activity of TC166 was associated with better OS, whereas the higher activities of
253 TC121, TC247, TC250, TC76, and TC146, were associated with worse OS. The top genes from
254 TC166 were enriched for genes involved in replication and apoptosis. The chromosomal
255 region 13q12-q14 linked to the TC166, contains the tumor suppressor genes retinoblastoma
256 1 (*RB1*) and Breast Cancer Type 2 Susceptibility Protein (*BRCA2*). Loss of heterozygosity of
257 this chromosomal region is frequently observed in both sporadic and hereditary serous
258 ovarian cancers (26,27). The top genes from TC247 were enriched for genes involved in
259 proliferation and immune cell activation, TC76 in replication stress, TC250 in extracellular
260 matrix (ECM) interactions, and TC146 in neurotransmitter signaling.
261 Intriguingly, the top 100 genes in TC121 revealed a co-functional cluster enriched for
262 genes involved in synaptic signaling, with the corresponding proteins reported to localize to
263 the synaptic membrane of neurons (Fig. 4). Among these were pre-synaptic protein

264 neurexin-1 (*NRXN1*) and its post-synaptic ligand leucine-rich repeat transmembrane protein
265 2 (*LRRTM2*), which regulates excitatory synapse formation (top 20 genes are described in
266 Supplementary Table S8, for more details: http://transcriptional-landscape-
267 ovarian.opendatainscience.net) (28,29). Furthermore, this co-functional cluster included
268 neuron-specific synaptic structure proteins, neurofilament light, and medium chain.
269 Moreover, genes encoding for potassium ion channel proteins integral to membrane
270 repolarization during synapse signal transduction carried high weights in TC121. These genes
271 included *KCNC1*, *KCNN2*, and *KCNIP1*(30–32). Several genes in TC121 encoded proteins
272 related to glutamate receptor signaling, including *GRIN2C* and *SLC7A10* (33). In line with this
273 proposed function, high activity of TC121 was observed in neuroblastoma cell lines but not
274 in ovarian or central nervous system cancer cell lines in the GDSC and CCLE datasets (Fig. 5A,
275 Supplementary Fig. S6, S7). In the GEO and TCGA datasets, high activity of TC121 was
276 observed in glioblastoma multiforme and lower-grade glioma but not in ovarian cancer
277 patient samples (Fig. 5B).
278
279 **Distinct spatial profiles of transcriptional components associated with overall survival**
280 Cross-study TC projection onto spatial transcriptomic profiles from 11 ovarian cancer
281 samples revealed that TC121 was highly active in profiles from the tumor region of the 11
282 ovarian cancer samples (Fig. 6A; Supplementary Fig. S8). Distinct regions with high activity of
283 the copy number TCs (TC166, TC247, and TC76) in the HGSOC sample overlapped with the
284 region containing cancer cells, as expected. TC250, enriched for extracellular matrix
285 interactions, was also active in the stromal region. The strongest inverse colocalization
286 (colocalization score -2.43) was observed between the activity scores of TC146, enriched for
287 neurotransmitter signaling, and TC76, captured the effect of copy number alterations at

288 chromosome 9p13-p21, at the serous ovarian cancer sample (Fig. 6B, Supplementary Table
289 S9).
290

291 ## Discussion

292 In this study, we identified 374 TCs, each enriched for gene sets representing various
293 biological processes in HGSOC samples. Six could stratify patients with HGSOC who had
294 received platinum-based treatment into ten distinct OS groups.

295 The most significant TC in the survival tree analysis, TC121, captured a clinically
296 relevant subtle transcriptional pattern linked to synaptic signaling not previously recognized
297 in HGSOC. In the survival tree, TC121 identified 12% of the HGSOC patients with the shortest
298 OS and, based on spatially resolved transcriptomic analyzed samples, is active in tumor
299 regions. This observation supports the emerging role of neurons and neuronal projections as
300 cancer hallmark-inducing constituents of the TME (34–36).

301 Further investigation on whether the activity of TC121 originated from tumor cells or
302 in the TME revealed that the TC121 signal is coming from cells within the TME. The high
303 activity of TC121 in low-grade glioma and glioblastoma multiforme patient samples (Fig. 5B)
304 is in agreement with the presence of neurons in large numbers within the TME of gliomas,
305 where they form functional synapses with tumor cells (37,38). Moreover, TC121 activity was
306 lower in non-brain cancers, such as ovarian cancers, which contain fewer neurons and
307 synapses in the TME compared to brain cancers. We expected TC121 activity to be low in the
308 bulk transcriptomes of all cell lines, since they lack TME. TC121 activity in most cell lines,
309 which includes glioblastoma and ovarian cancer cell lines, was indeed low. Neuroblastoma
310 cell lines, however, exhibited high TC121 activity, which is likely due to retained synaptic
311 formation capacity originating from neuroblast cells (39,40). Lastly, TC121's high activity

312 observed in small, scattered regions within the tumor of spatially resolved transcriptomic
313 ovarian cancer samples also supports TC121's role in the TME.

314 TC121's significant association with OS underscores the potential significance of
315 synaptic signaling in HGSOC biology. Yet, the neuronal subtype and the molecular
316 mechanisms associated with TC121 remain to be elucidated. A study in human ovarian
317 cancer-bearing mice demonstrated that sympathetic innervation in HGSOC involves
318 adrenergic signaling: norepinephrine released by sympathetic neurons binds to beta-
319 adrenergic receptors on the cancer cells (41–43). This binding triggers the tumor cells to
320 release brain-derived neurotrophic factor (BDNF), which enhances cancer innervation via
321 activation of host neurotrophic receptor tyrosine kinase B receptors, thereby establishing a
322 feed-forward loop of sustained signaling. BDNF and the nerve marker neurofilament protein
323 expression were examined in 108 human ovarian tumors (41). This study revealed that
324 increased intratumoral nerve presence strongly correlates with elevated BDNF and
325 norepinephrine levels, advanced tumor stage, and shorter OS in patients with ovarian
326 cancer. Our analysis indicated that *BDNF* is a prominent gene (with an absolute weight > 3)
327 in 10 TCs but not in TC121, suggesting that TC121 may indicate a distinct process unrelated
328 to BDNF.

329 The significance of sensory innervation in HGSOC was evidenced by the co-
330 localization of TRPV1, a marker for sensory neurons, and β-III tubulin, a general neuronal
331 marker, in immunofluorescent staining of histological sections from 75 patients (44).
332 Additionally, a murine model study employing neural tracing identified sensory neurons
333 originating from local dorsal root ganglia and jugular–nodose ganglia, with axons extending
334 into the TME (44). A transgenic murine model lacking nociceptors demonstrated that this
335 specific subtype of sensory neurons was involved in tumor progression (45). Another study

336 showed that reducing the release of Calcitonin gene-related peptide from tumor-innervating
337 nociceptors could be a strategy to alleviate this effect of nociceptors by improving anti-
338 tumour immunity of cytotoxic CD8+ T cells in a melanoma model bearing mice (46). This
339 indicates that the signal from TC121 may represent an indirect influence on tumor cells via
340 interactions with immune cells and the promotion of an immune suppressive TME.
341 Furthermore, in cell lines derived from Trp53$^{-/-}$ Pten$^{-/-}$ murine HGSOC, the influence of
342 nociceptors was characterized by the release of substance P (SP), their primary
343 neuropeptide. SP is an alternative splicing product of the preprotachykinin A gene (*TAC1*)
344 and binds to the receptor neurokinin 1 (NK1R), encoded by the *TACR1* gene. NK1R
345 expression was confirmed in murine HGSOC cell line, and SP enhanced cellular proliferation
346 in NK1R-positive murine HGSOC cancer cells *in vitro* (45). Our analysis identified *TAC1* and
347 *TACR1* as prominent genes in 15 and 2 TCs, respectively, yet not in TC121, and none of these
348 TCs were associated with patient survival. Currently, there are no drugs specifically targeting
349 tumor innervation in (ovarian) cancer (47). Interestingly, the NK1R antagonist aprepitant
350 effectively inhibited the metastasis-promoting effects of neural substance P in human breast
351 and mammary cancer bearing mice (48), demonstrating the feasibility of such an approach.
352 Therefore, it is essential that the mechanisms driving this nerve growth, the specifics of how
353 nerves within the TME interact with ovarian cancer cells, and how they impact the survival of
354 patients with HGSOC are further elucidated.

355 Altogether, the present study uncovered a clinically relevant TC linked to synaptic
356 signaling not previously identified in HGSOC. This TC may represent a novel cancer cell-
357 extrinsic mechanism within the TME, illustrating how cancer cells and nerve cells interact to
358 promote enhanced proliferation. A deeper understanding of the molecular aspects of tumor
359 innervation could pave the way for novel drug targets for patients with HGSOC.

Data availability

Microarray expression data was collected from three public data repositories: Gene Expression Omnibus with accession number GPL570 (generated with Affymetrix HG-U133 Plus 2.0), CCLE (generated with Affymetrix HG-U133 Plus 2.0, file CCLE_Expression.Arrays_2013-03-18.tar.gz) available at https://portals.broadinstitute.org/ccle/data and GDSC (generated with Affymetrix HG-U219) available at https://www.ebi.ac.uk/arrayexpress/experiments/E-MTAB-3610/. Pre-processed and normalized RNA-seq data was collected from TCGA using the Broad GDAC Firehose portal (https://gdac.broadinstitute.org/). Spatially resolved samples were sourced from 10xGenomics and GEO. The datasets generated during and/or analyzed during the current study are available in the website: http://transcriptional-landscape-ovarian.opendatainscience.net.

Funding

This research was supported by a Hanarth Fund grant, the Netherlands (2019N1552 to R.S.N.F).

Author contribution

A. Bhattacharya: Data curation, methodology, data analysis, data interpretation, writing. T. S. Stutvoet: Data curation, methodology, data analysis, data interpretation, writing. M. Perla: Data interpretation, writing. S. Loipfinger: Data analysis, data interpretation, writing. M. Jalving: Data interpretation, writing. A. K. L. Reyners: Data interpretation, writing. P. D. Vermeer: Data interpretation, writing. R. Drapkin: Data interpretation, writing. M. de Bruyn:

383 Data interpretation, writing. E. G. E. de Vries: Data interpretation, writing. S. de Jong:
384 Conceptualization, data interpretation, writing. R. S. N. Fehrmann: Conceptualization, data
385 curation, methodology, data analysis, data interpretation, writing. All were involved in the
386 final decision to submit the manuscript.
387

388 ## Disclosure

389 The authors have declared no conflicts of interest.
390

391 ## Figure legends

392 **Figure 1.** Workflow indicates the data acquisition and relations between the methods.
393

394 **Figure 2.** Enrichment heatmap of Hallmark gene sets in each TC associated with patient OS.
395 GSEA results of 14 TCs associated with OS in univariate or multivariate survival analysis are
396 presented, including Hallmark gene sets that were included in the enrichment for at least
397 one TC that passed the Bonferroni threshold for multiple testing correction. The gene sets
398 were clustered using Pearson correlation and Ward D2, and the heatmap colors were based
399 on Z-scores, truncated at a value of four. The right column shows the chromosomal location
400 of a copy number alteration that the TC captures the downstream effects on gene
401 expression levels.
402

403 **Figure 3**. Survival tree analysis of patients with platinum-treated HGSOC defines survival
404 cohorts with distinct clinicopathologic and biological characteristics. Survival tree analysis of
405 294 patients with platinum-treated HGSOC using 14 OS-associated TCs and other classifiers

406 such as age, tumor stage, grade, and debulking status. The analysis resulted in nine survival
407 cohorts, and the height of the bar in the Sankey diagram represents the number of patients
408 in each cohort. The Kaplan-Meier plots and number-at-risk tables are presented with survival
409 data censored at 10 years. The names of the survival cohorts were based on enriched
410 biological processes in the TCs, as determined by the chromosomal location of genes
411 captured by a TC, GSEA, and co-functionality analysis of the top genes. The p-values in each
412 panel show the p-value from the corresponding log-rank test between the two groups.
413 Abbreviations: TC = transcriptional component, ECM = extracellular matrix.
414
415 **Figure 4**. Co-functionality network of top 100 absolute weighted genes in TC121. One
416 cluster with more than 5 genes was identified in both Gene ontology biological processes
417 and cellular components databases having strong shared predicted co-functionality
418 ($r > 0.7$). This cluster shows high enrichment for genes related to the synaptic signaling in
419 the Gene ontology biological processes database and synaptic membrane in the cellular
420 components database.
421
422 **Figure 5.** The activity of TC121 in bulk transcriptomes of CCLE, GDSC cell lines, and GEO and
423 TCGA patient-derived samples. **A.** Cross-study TC projection of TC121 on CCLE and GDSC cell
424 lines. The boxplots display the activity scores of TC121 in different tissue types, which are
425 ordered based on their corresponding median activity scores. **B**. Cross-study TC projection of
426 TC121 on GEO and TCGA bulk transcriptomes resulted in the activity scores presented in the
427 boxplots. Cancer types were ordered based on corresponding medians of TC121 activity
428 scores. Abbreviations: TC = transcriptional component.
429

430 **Figure 6.** Spatial transcriptomic profiles in ovarian cancer samples. **A.** We employed a
431 permutation-based approach to pinpoint the areas of significant TC activity in spatial
432 transcriptomic profiles. We ran 5,000 permutations for each TC-profile combination, yielding
433 a p-value that indicates the extent to which the TC activity in the corresponding profile
434 differs from what would be expected by chance (the null distribution). We then transformed
435 these p-values into logarithmic values and represented them using a heatmap. Heatmaps of
436 activity scores of the TCs are presented in individual rows for the HGSOC, serous papillary,
437 and endometrioid adenocarcinoma of ovary samples. The first column represents the
438 stained images of the samples. The second to seventh columns show heatmaps
439 corresponding to the mentioned TCs. **B.** The heatmap illustrates the colocalization between
440 two TC activities on spatial transcriptomic profiles from ovarian cancer samples. For each
441 cell, the colocalization scores of the TCs at each of the three spatial transcriptomics samples
442 OC 1, OC 2, and OC 3 are arranged in columns. A colocalization score of 4 between two TCs
443 (red) indicates that the positively (+) and negatively (-) active regions of both TCs are
444 perfectly colocalized. Conversely, a colocalization score of -4 between two TCs (blue) also
445 indicates colocalization. Still, with inverse activity, i.e., the positively active regions of one TC
446 are colocalized with the negatively active regions of the other TC or vice versa. A
447 colocalization score close to 0 between two TCs (white) indicates that the activities of two
448 TCs are spatially separated. The dashed and solid circle in the panel on the right side of the
449 color bar represents two different TCs. Abbreviations: TC = transcriptional component.
450
451 **Supplementary Figure S1.** Association of OS-related TCs with clinicopathologic parameters.
452 The association between clinicopathologic parameters and the activity of the OS-associated
453 14 TCs was determined in the complete set of 1,125 samples. Pearson correlation was used

454 to calculate the association of each clinicopathologic parameter with each TC. The TCs were
455 then ranked based on their association with OS. Abbreviations: TC = transcriptional
456 component, OS = overall survival.
457
458 **Supplementary Figure S2.** Enrichment heatmap for the KEGG gene set collection in OS-
459 related TCs. GSEA results of 14 TCs associated with OS in univariate or multivariate survival
460 analysis are presented, including KEGG gene sets that were included if the enrichment for at
461 least one TC passed the Bonferroni threshold for multiple testing correction. The gene sets
462 were clustered using Pearson correlation and Ward D2, and the heatmap colors were based
463 on Z-scores, truncated at a value of four. The right column shows the chromosomal location
464 of a copy number alteration that the TC captures the downstream effects on gene
465 expression levels. Abbreviations: TC = transcriptional component, OS = overall survival.
466
467 **Supplementary Figure S3.** Enrichment heatmap for the REACTOME gene set collection in OS-
468 related TCs. GSEA results of 14 TCs associated with OS in univariate or multivariate survival
469 analysis is presented, including REACTOME gene sets that were included if the enrichment
470 for at least one TC passed the Bonferroni threshold for multiple testing correction. The gene
471 sets were clustered using Pearson correlation and Ward D2, and the heatmap colors were
472 based on Z-scores, truncated at a value of four. The right column shows the chromosomal
473 location of a copy number alteration that the TC captures the downstream effects on gene
474 expression levels. Abbreviations: TC = transcriptional component.
475

476 **Supplementary Figure S4.** Survival tree analysis of patients with advanced-stage, HGSOC
477 defines survival cohorts with distinct clinicopathologic and biological characteristics. Survival
478 tree analysis of 265 patients with advanced-stage, platinum-treated HGSOC using 14 OS-
479 associated TCs and other classifiers such as age, tumor stage, grade, and debulking status.
480 The analysis resulted in nine survival cohorts, and the height of the bar in the Sankey
481 diagram represents the number of patients in each cohort. The Kaplan-Meier plots and
482 number-at-risk tables are presented with survival data censored at 10 years. The names of
483 the survival cohorts were based on enriched biological processes in the TCs, as determined
484 by the chromosomal location of genes captured by a TC, GSEA, and co-functionality analysis
485 of the top genes. The p-values in each panel show the p-value from the corresponding log-
486 rank test between the two groups. Abbreviations: TC = transcriptional component, ECM =
487 extracellular matrix.
488
489 **Supplementary Figure S5.** Three OS-associated TCs capture the transcriptional effect of copy
490 number alterations. For each OS-related TC, the weight of each gene was plotted on its
491 genomic location. Abbreviations: TC = transcriptional component.
492
493 **Supplementary Figure S6**. Activity of OS-associated TCs in bulk transcriptomes of CCLE cell
494 lines. The proportion of samples with outlier activity scores in individual tissue types for each
495 of the 14 OS-associated TCs was obtained using an absolute cut-off value of 0.05. TCs were
496 ordered based on their association with OS. Abbreviations: TC = transcriptional component.
497
498 **Supplementary Figure S7**. The activity of OS-associated TCs in bulk transcriptomes of GDSC
499 cell lines. The proportion of samples with outlier activity scores in individual tissue types for

500 each of the 14 OS-associated TCs was obtained using an absolute cut-off value of 0.05. TCs
501 were ordered based on their association with OS. Abbreviations: TC = transcriptional
502 component.

503

504 **Supplementary Figure S8**. Spatial transcriptomic profiles in eight ovarian cancer samples. **A.**
505 We employed a permutation-based approach to pinpoint the areas of significant TC activity
506 in spatial transcriptomic profiles. We ran 5,000 permutations for each TC-profile
507 combination, yielding a p-value that indicates the extent to which the TC activity in the
508 corresponding profile differs from what would be expected by chance (the null distribution).
509 We then transformed these p-values into logarithmic values and represented them using a
510 heatmap. Heatmaps of activity scores of the TCs are presented in individual rows for the
511 HGSOC samples. The first column represents the stained images of the samples. The second
512 to seventh columns show heatmaps corresponding to the mentioned TCs. **B.** The heatmap
513 illustrates the colocalization between two TC activities on spatial transcriptomic profiles
514 from ovarian cancer samples. For each cell, the colocalization scores of the TCs at each of
515 the eight spatial transcriptomics samples are arranged in columns. A colocalization score of 4
516 between two TCs (red) indicates that the positively (+) and negatively (-) active regions of
517 both TCs are perfectly colocalized. Conversely, a colocalization score of -4 between two TCs
518 (blue) also indicates colocalization. Still, with inverse activity, i.e., the positively active
519 regions of one TC are colocalized with the negatively active regions of the other TC or vice
520 versa. A colocalization score close to 0 between two TCs (white) indicates that the activities
521 of two TCs are spatially separated. The dashed and solid circle in the panel on the right side
522 of the color bar represents two different TCs. Abbreviations: TC = transcriptional component.

523

524 **Supplementary table legends**

525 **Supplementary Table S1.** Patient characteristics. Abbreviations: NA = not applicable, HGSOC
526 = high-grade serous ovarian cancer, LGSOC = low-grade serous ovarian cancer, LMP = low
527 malignant potential, OCCC = ovarian clear cell cancer.

528

529 **Supplementary Table S2.** Overview of the number of samples from each GEO series and the
530 corresponding study. Abbreviations: PMID = PubMed identification number.

531

532 **Supplementary Table S3.** Multivariate permutation framework results from the univariate
533 survival analysis. Abbreviations: TC = transcriptional component. CI = confidence interval

534

535 **Supplementary Table S4.** Permutation framework results from the multivariate survival
536 analysis. Abbreviations: TC = transcriptional component. CI = confidence interval

537

538 **Supplementary Table S5.** Clinicopathological parameters per survival tree node in platinum-
539 treated HGSOC. Abbreviations: HGSOC = high-grade serous ovarian cancer, TC =
540 transcriptional component, ECM = extracellular matrix.

541

542 **Supplementary Table S6.** Clinicopathological parameters per survival tree node in advanced-
543 stage platinum-treated HGSOC. Abbreviations: HGSOC = high-grade serous ovarian cancer,
544 TC = transcriptional component, ECM = extracellular matrix.

545

546 **Supplementary Table S7.** GenetICA gene network analysis results. Abbreviations: TC =
547 transcriptional component.

548

549 **Supplementary Table S8.** Expression and function of the top 20 genes in TC121, according to

550 literature. Abbreviations: TC = transcriptional component.

551

552 **Supplementary Table S9.** Colocalization scores of every two TC combinations in spatial

553 transcriptomic profiles from three ovarian cancer samples. Abbreviations: TC =

554 transcriptional component.

555 **References**

556

557 1. Lheureux S, Gourley C, Vergote I, Oza AM. Epithelial ovarian cancer. *Lancet*
558 2019;393:1240–53.

559 2. NCCN clinical practice guidelines in oncology - ovarian cancer, including fallopian tube
560 cancer and primary peritoneal cancer. November 26, 2019.

561 3. Wright AA, Bohlke K, Armstrong DK, Bookman MA, Cliby WA, Coleman RL, et al.
562 Neoadjuvant chemotherapy for newly diagnosed, advanced ovarian cancer: Society of
563 Gynecologic Oncology and American Society of Clinical Oncology Clinical Practice Guideline. *J*
564 *Clin Oncol* 2016;34:3460–73.

565 4. Corrado G, Salutari V, Palluzzi E, Distefano MG, Scambia G, Ferrandina G. Optimizing
566 treatment in recurrent epithelial ovarian cancer. *Expert Rev Anticancer Ther* 2017;17:1147–
567 58.

568 5. Cibula D, Balmaña J. PARP inhibitors in ovarian cancer. *Ann Oncol* 2016;27:i40–44.

569 6. Wang H, Xu T, Zheng L, Li G. Angiogenesis inhibitors for the treatment of ovarian cancer.
570 *Int J Gynecol Cancer* 2018;28:903–14.

571 7. Wu SG, Wang J, Sun JY, He ZY, Zhang WW, Zhou J. Real-world impact of survival by period
572 of diagnosis in epithelial ovarian cancer between 1990 and 2014. *Front Oncol* 2019;9:639.

573 8. Tewari KS, Burger RA, Enserro D, Norquist BM, Swisher EM, Brady MF, et al. Final overall
574 survival of a randomized trial of Bevacizumab for primary treatment of ovarian cancer. *J Clin*
575 *Oncol* 2019;37:2317–28.

576 9. Bell D, Berchuck A, Birrer M, Chien J, Cramer DW, Dao F, et al. Integrated genomic
577 analyses of ovarian carcinoma. *Nature* 2011;474:609–15.

578 10. Tothill RW, Tinker AV, George J, Brown R, Fox SB, Lade S, et al. Novel molecular subtypes
579 of serous and endometrioid ovarian cancer linked to clinical outcome. *Clin Cancer Res*
580 2008;14:5198–208.

581 11. Verhaak RGW, Tamayo P, Yang JY, Hubbard D, Zhang H, Creighton CJ, et al. Prognostically
582 relevant gene signatures of high-grade serous ovarian carcinoma. *J Clin Investig*
583 2013;123:517–25.

584 12. Chen C, Grennan K, Badner J, Zhang D, Gershon E, Jin L, et al. Removing batch effects in
585 analysis of expression microarray data: an evaluation of six batch adjustment methods. *PLoS*
586 *One* 2011;6:e17238.

587 13. Kong W, Vanderburg CR, Gunshin H, Rogers JT, Huang X. A review of independent
588 component analysis application to microarray gene expression data. *BioTechniques*
589 2008;45:501–20.

590 14. Chiappetta P, Roubaud MC, Torrsani B. Blind source separation and the analysis of
591 microarray data. *J Comput Biol* 2004;11:1090–109.

592 15. Biton A, Bernard-Pierrot I, Lou Y, Krucker C, Chapeaublanc E, Rubio-Pérez C, et al.
593 Independent component analysis uncovers the landscape of the bladder tumor
594 transcriptome and reveals insights into luminal and basal subtypes. *Cell Rep* 2014;9:1235–45.

595 16. Clough E, Barrett T. Statistical genomics, methods and protocols. *Methods Mol Biol*
596 2016;1418:93–110.

597 17. Fehrmann RSN, Karjalainen JM, Krajewska M, Westra H-J, Maloney D, Simeonov A, et al.
598 Gene expression analysis identifies global gene dosage sensitivity in cancer. *Nat Genet*
599 2015;47:115–25.

600 18. Barretina J, Caponigro G, Stransky N, Venkatesan K, Margolin AA, Kim S, et al. The cancer
601 cell line encyclopedia enables predictive modelling of anticancer drug sensitivity. *Nature*
602 2012;483:603–7.

603 19. Yang W, Soares J, Greninger P, Edelman EJ, Lightfoot H, Forbes S, et al. Genomics of drug
604 sensitivity in Cancer (GDSC): a resource for therapeutic biomarker discovery in cancer cells.
605 *Nucleic Acids Res* 2013;41:D955–61.

606 20. Barrett T, Wilhite SE, Ledoux P, Evangelista C, Kim IF, Tomashevsky M, et al. NCBI GEO:
607 archive for functional genomics data sets—update. *Nucleic Acids Res* 2013;41:D991–5.

608 21. Bhattacharya A, Bense RD, Urzúa-Traslaviña CG, de Vries EGE, van Vugt MATM,
609 Fehrmann RSN. Transcriptional effects of copy number alterations in a large set of human
610 cancers. *Nat Commun* 2020;11:715.

611 22. Subramanian A, Tamayo P, Mootha VK, Mukherjee S, Ebert BL, Gillette MA, et al. Gene
612 set enrichment analysis: a knowledge-based approach for interpreting genome-wide
613 expression profiles. *Proc Natl Acad Sci* 2005;102:15545–50.

614 23. Köhler S, Carmody L, Vasilevsky N, Jacobsen JOB, Danis D, Gourdine J-P, et al. Expansion
615 of the human phenotype ontology (HPO) knowledge base and resources. *Nucleic Acids Res*
616 2019;47(D1):D1018-D1027.

617 24. Urzúa-Traslaviña CG, Leeuwenburgh VC, Bhattacharya A, Loipfinger S, van Vugt MATM,
618 de Vries EGE , et al. Improving gene function predictions using independent transcriptional
619 components. *Nat Commun* 2021;12:1464.

620 25. Canozo FJG, Zuo Z, Martin JF, Samee MdAH. Cell-type modeling in spatial transcriptomics
621 data elucidates spatially variable colocalization and communication between cell-types in
622 mouse brain. *Cell Syst* 2022;13:58-70.e5.

623 26. Huang RY, Chen GB, Matsumura N, Lai HC, Mori S, Li J, et al. Histotype-specific copy-
624 number alterations in ovarian cancer. *BMC Méd Genom* 2012;5:47.

625 27. Jongsma APM, Piek JMJ, Zweemer RP, Verheijen RHM, Gebbinck JWTK, Kamp GJ van, et
626 al. Molecular evidence for putative tumour suppressor genes on chromosome 13q specific to
627 BRCA1 related ovarian and fallopian tube cancer. *Mol Pathol* 2002;55:305.

628 28. Ko J, Fuccillo MV, Malenka RC, Südhof TC. LRRTM2 functions as a neurexin ligand in
629 promoting excitatory synapse formation. *Neuron* 2009;64:791–8.

630 29. de Wit J, Sylwestrak E, O'Sullivan ML, Otto S, Tiglio K, Savas JN, et al. LRRTM2 interacts
631 with neurexin1 and regulates excitatory synapse formation. *Neuron* 2009;64:799–806.

632 30. Ried T, Rudy B, Miera EV-S de, Lau D, Ward DC, Sen K. Localization of a highly conserved
633 human potassium channel gene (NGK2-KV4; KCNC1) to chromosome 11p15. *Genomics*
634 1993;15:405–11.

635 31. Willis M, Trieb M, Leitner I, Wietzorrek G, Marksteiner J, Knaus H-G. Small-conductance
636 calcium-activated potassium type 2 channels (SK2, KCa2.2) in human brain. *Brain Struct*
637 *Funct* 2017;222:973–9.

638 32. Bourdeau ML, Laplante I, Laurent CE, Lacaille JC. KChIP1 modulation of Kv4.3-mediated
639 A-type K+ currents and repetitive firing in hippocampal interneurons. *Neuroscience*
640 2011;176:173–87.

641 33. Ehmsen JT, Liu Y, Wang Y, Paladugu N, Johnson AE, Rothstein JD, et al. The astrocytic
642 transporter SLC7A10 (Asc-1) mediates glycinergic inhibition of spinal cord motor neurons. *Sci*
643 *Rep* 2016;6:35592.

644 34. Hanahan D, Weinberg RA. Hallmarks of cancer: the next generation. *Cell* 2011;144:646–
645 74.

646 35. Reavis HD, Chen HI, Drapkin R. Tumor Innervation: Cancer Has Some Nerve. *Trends*
647 *Cancer* 2020;6:1059–67.

648 36. Gysler SM, Drapkin R. Tumor innervation: peripheral nerves take control of the tumor
649 microenvironment. *J Clin Investig* 2021;131:e147276.

650 37. Radin DP, Tsirka SE. Interactions between tumor cells, neurons, and microglia in the
651 glioma microenvironment. *Int J Mol Sci* 2020;21:8476.

652 38. Venkatesh HS, Morishita W, Geraghty AC, Silverbush D, Gillespie SM, Arzt M, et al.
653 Electrical and synaptic integration of glioma into neural circuits. *Nature* 2019;573:539–45.

654 39. Preter KD, Vandesompele J, Heimann P, Yigit N, Beckman S, Schramm A, et al. Human
655 fetal neuroblast and neuroblastoma transcriptome analysis confirms neuroblast origin and
656 highlights neuroblastoma candidate genes. *Genome Biol* 2006;7:R84.

657 40. Mark B, Lai S-L, Zarin AA, Manning L, Pollington HQ, Litwin-Kumar A, et al. A
658 developmental framework linking neurogenesis and circuit formation in the Drosophila CNS.
659 *eLife* 2021;10:e67510.

660 41. Allen JK, Armaiz-Pena GN, Nagaraja AS, Sadaoui NC, Ortiz T, Dood R, et al. Sustained
661 adrenergic signaling promotes intratumoral innervation through BDNF induction. *Cancer Res*
662 2018;78:3233-3242.

663 42. Rains SL, Amaya CN, Bryan BA. Beta-adrenergic receptors are expressed across diverse
664 cancers. *Oncoscience* 2017;4:95–105.

665 43. Eng JWL, Kokolus KM, Reed CB, Hylander BL, Ma WW, Repasky EA. A nervous tumor
666 microenvironment: the impact of adrenergic stress on cancer cells, immunosuppression, and
667 immunotherapeutic response. *Cancer Immunol Immunother* 2014;63:1115–28.

668 44. Barr JL, Kruse A, Restaino AC, Tulina N, Stuckelberger S, Vermeer SJ, et al. Intra-tumoral
669 nerve-tracing in a novel syngeneic model of high-grade serous ovarian carcinoma. *Cells*
670 2021;10:3491.

671 45. Restaino AC, Walz A, Vermeer SJ, Barr J, Kovács A, Fettig RR, et al. Functional neuronal
672 circuits promote disease progression in cancer. *Sci Adv* 2023;9:eade4443.

673 46. Balood M, Ahmadi M, Eichwald T, Ahmadi A, Majdoubi A, Roversi K, et al. Nociceptor
674 neurons affect cancer immunosurveillance. Nature. 2022;611:405–12.

675 47. Li X, Peng X, Yang S, Wei S, Fan Q, Liu J, et al. Targeting tumor innervation: premises,
676 promises, and challenges. *Cell Death Discov* 2022;8:131.

677 48. Padmanaban V, Keller I, Seltzer ES, Ostendorf BN, Kerner Z, Tavazoie SF. Neuronal
678 substance-P drives breast cancer growth and metastasis via an extracellular RNA-TLR7 axis.
679 *bioRxiv* 2024;2024.03.08.584128.

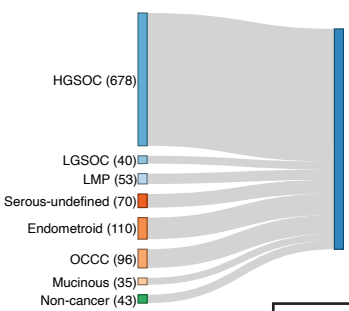

bulk transcriptomics (n = 1,125)

$$\begin{bmatrix} x_1 \\ x_2 \\ \vdots \\ x_n \end{bmatrix}$$

Consensus independent component analysis

$f(u) = \log \cosh(u)$

Mixing matrix (TC activity per sample)

$$\begin{bmatrix} \hat{a}_{11} & \hat{a}_{21} & \cdots & \hat{a}_{n1} \\ \hat{a}_{12} & \hat{a}_{22} & \cdots & \hat{a}_{n2} \\ \vdots & \vdots & & \vdots \\ \hat{a}_{1m} & \hat{a}_{2m} & \cdots & \hat{a}_{nm} \end{bmatrix}$$

Transcriptional components (Gene weights in TC)

$$\begin{bmatrix} \hat{s}_1 \\ \hat{s}_2 \\ \vdots \\ \hat{s}_m \end{bmatrix}$$

Cox proportional hazards analysis for OS

Univariate

TC activity scores

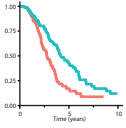

Multivariate

TC activity scores
Age
Stage
Grade
Debulking status

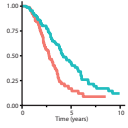

TCs significantly associated with OS after multiple testing correction

Survival tree analysis on platinum treated serous ovarian cancer patients

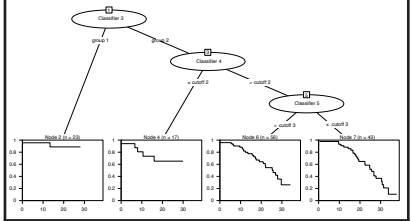

Robustness analysis using permutations

Identification of biological processes related to clinical outcome

TC activity↑

↓

Expression of genes in biological processes↑

↓

Overall survival↓

Association with biological processes

GenetICA-Network analysis

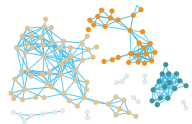

Geneset enrichment analysis on 16 geneset databases

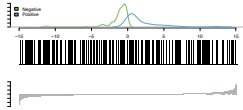

Copy number detection

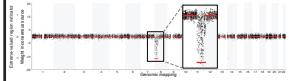

Cross-study TC projection

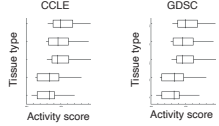

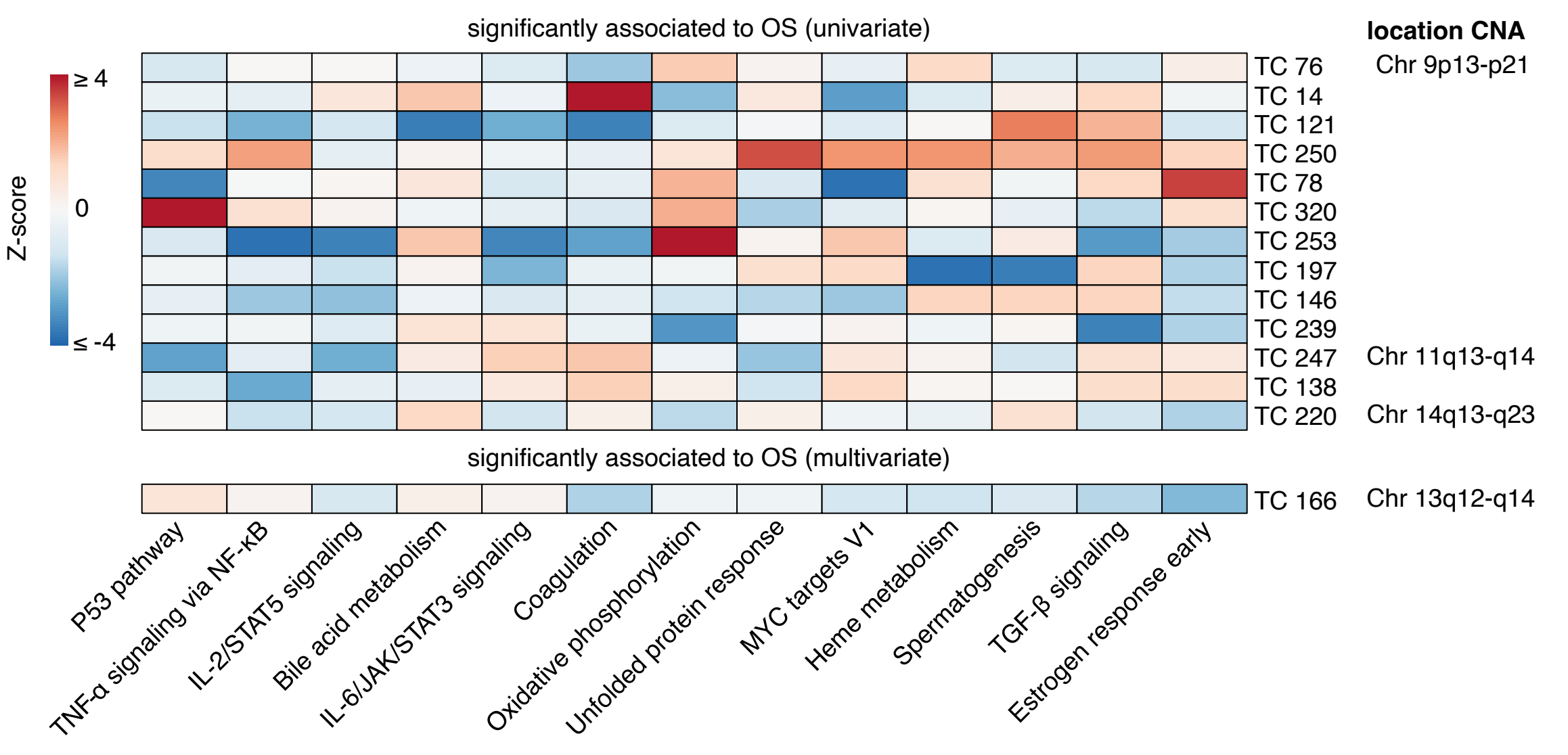
significantly associated to OS (univariate)
location CNA
Z-score
≥ 4
0
≤ -4
TC 76
TC 14
TC 121
TC 250
TC 78
TC 320
TC 253
TC 197
TC 146
TC 239
TC 247
TC 138
TC 220
Chr 9p13-p21
Chr 11q13-q14
Chr 14q13-q23
significantly associated to OS (multivariate)
TC 166
Chr 13q12-q14
P53 pathway
TNF-α signaling via NF-κB
IL-2/STAT5 signaling
Bile acid metabolism
IL-6/JAK/STAT3 signaling
Coagulation
Oxidative phosphorylation
Unfolded protein response
MYC targets V1
Heme metabolism
Spermatogenesis
TGF-β signaling
Estrogen response early

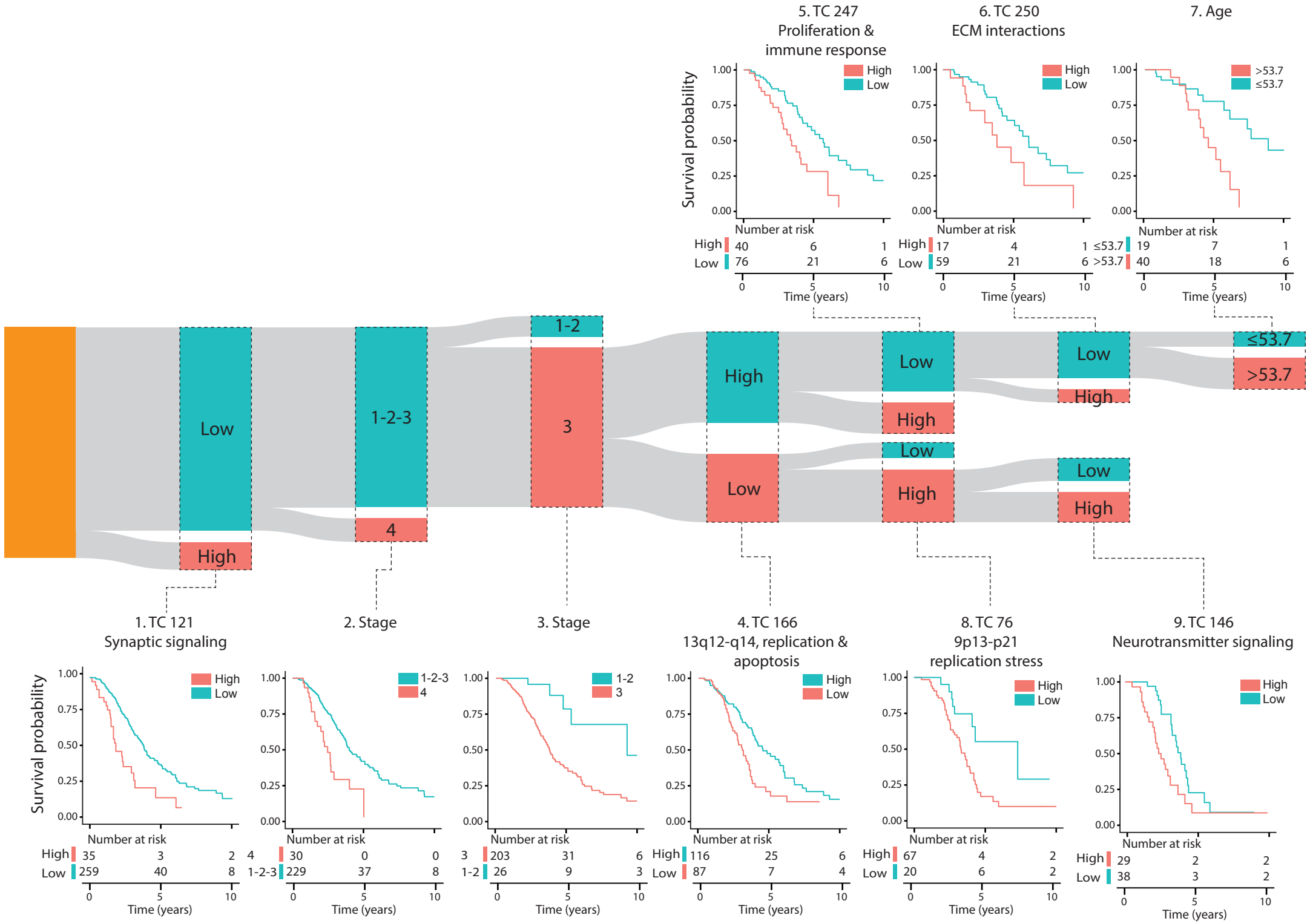
5. TC 247
Proliferation &
immune response
6. TC 250
ECM interactions
7. Age
Survival probability
High
Low
>53.7
≤53.7
Number at risk
High 40 6 1
Low 76 21 6
High 17 4 1
Low 59 21 6
≤53.7 19 7 1
>53.7 40 18 6
Time (years)
1-2
1-2-3
3
4
High
Low
1. TC 121
Synaptic signaling
2. Stage
3. Stage
4. TC 166
13q12-q14, replication &
apoptosis
8. TC 76
9p13-p21
replication stress
9. TC 146
Neurotransmitter signaling
High 35 3 2
Low 259 40 8
4 30 0 0
1-2-3 229 37 8
3 203 31 6
1-2 26 9 3
High 116 25 6
Low 87 7 4
High 67 4 2
Low 20 6 2
High 29 2 2
Low 38 3 2

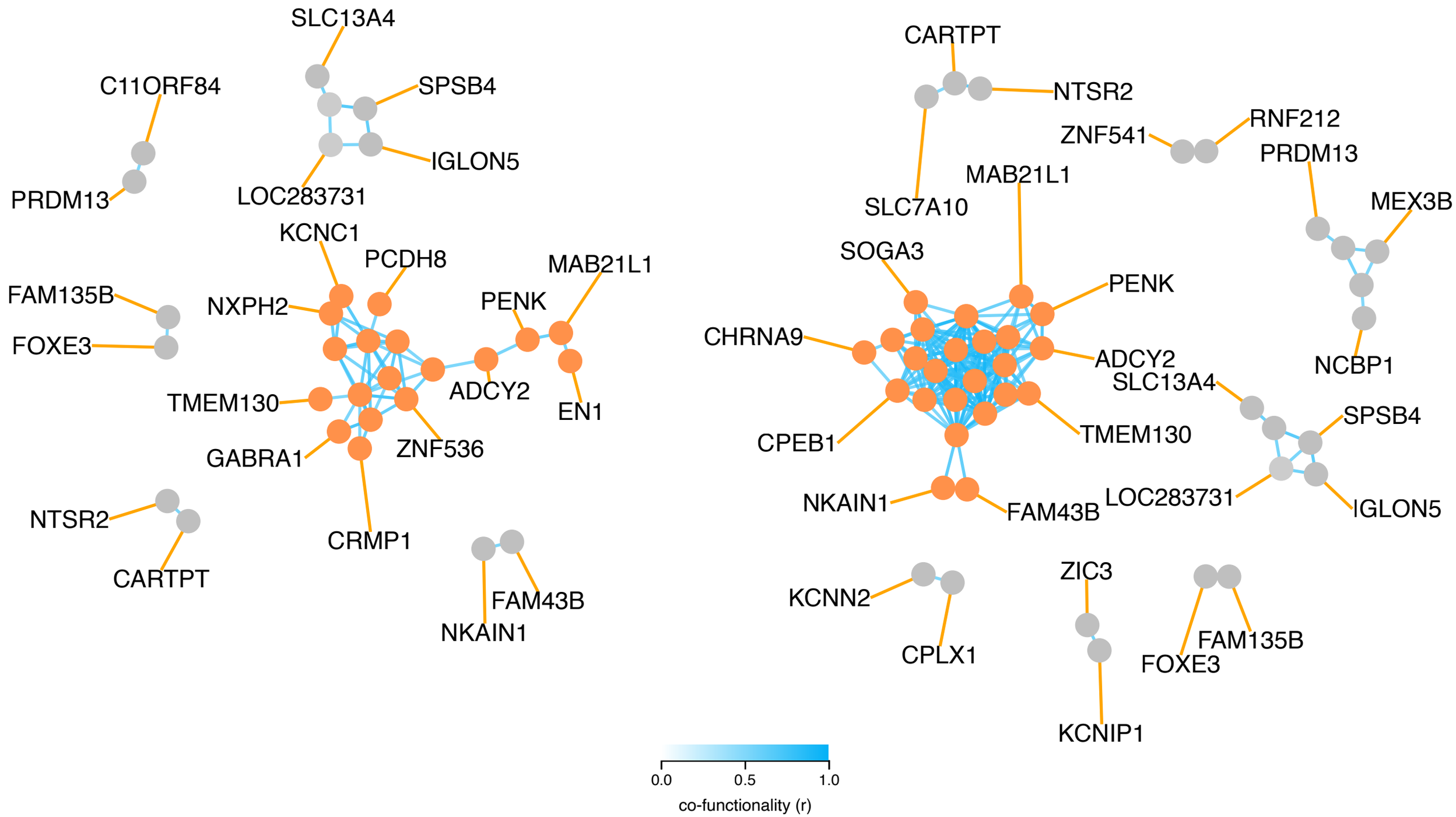

Z-score Gene Ontology biological processes genesets

- 11.5 - Synaptic signaling
- 10.3 - Modulation of synaptic transmission
- 9.51 - Single organism behavior
- 8.78 - Adult behavior
- 8.09 - Regulation of synaptic plasticity
- 7.69 - Cognition
- 7.47 - Glutamate receptor signaling
- 7.35 - Regulation of synaptic structure
- 7.34 - Behavior
- 7.12 - Regulation of neurotransmitter

Z-score Gene Ontology cellular components genesets

- 8.33 - Synaptic membrane
- 8.00 - Presynapse
- 7.72 - Postsynapse
- 7.61 - Postsynaptic membrane
- 7.57 - Presynaptic membrane
- 7.57 - Presynaptic active zone
- 7.43 - Transporter complex
- 7.08 - Potassium channel complex
- 7.07 - AMPA Glutamate receptor complex
- 7.03 - Cation channel complex

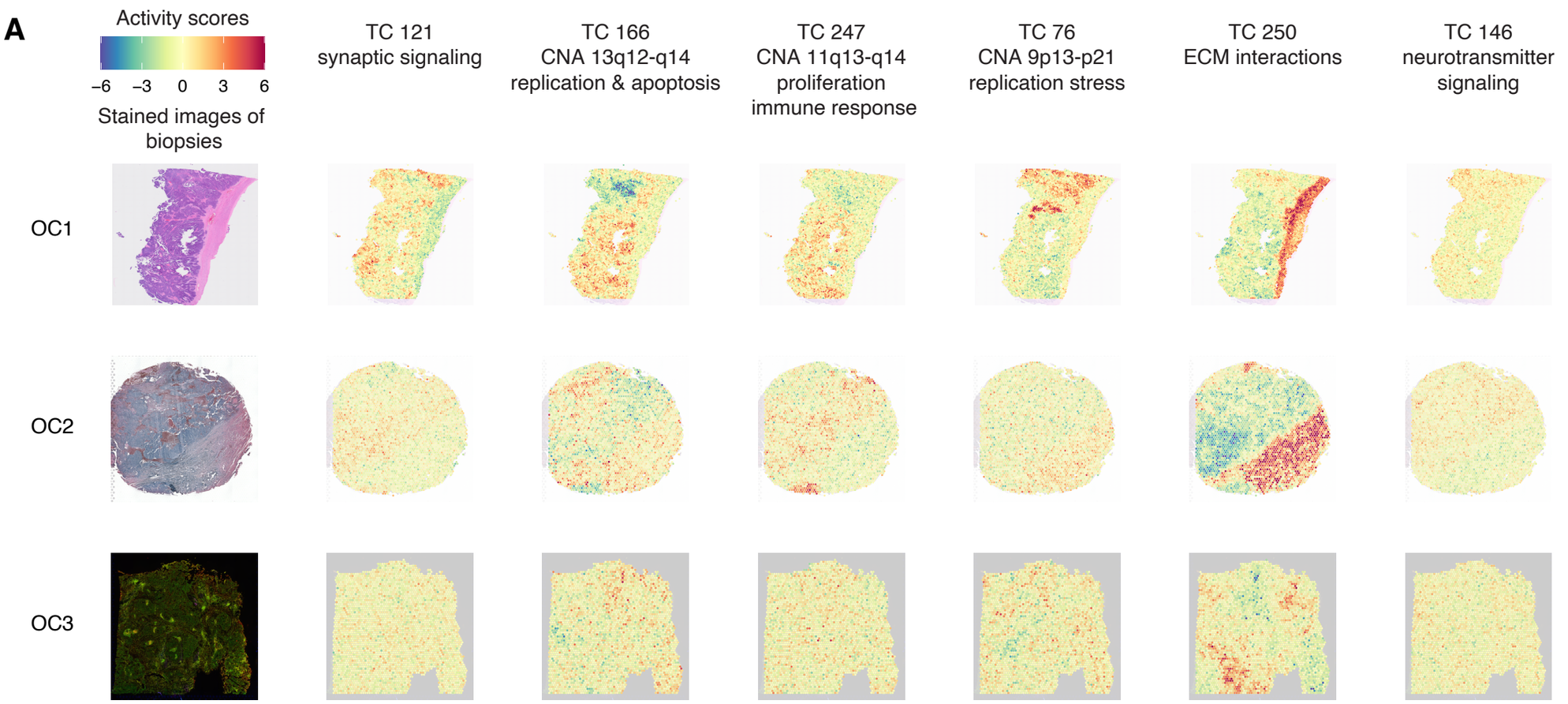
A
Activity scores
−6 −3 0 3 6
Stained images of biopsies
TC 121
synaptic signaling
TC 166
CNA 13q12-q14
replication & apoptosis
TC 247
CNA 11q13-q14
proliferation
immune response
TC 76
CNA 9p13-p21
replication stress
TC 250
ECM interactions
TC 146
neurotransmitter
signaling
OC1
OC2
OC3

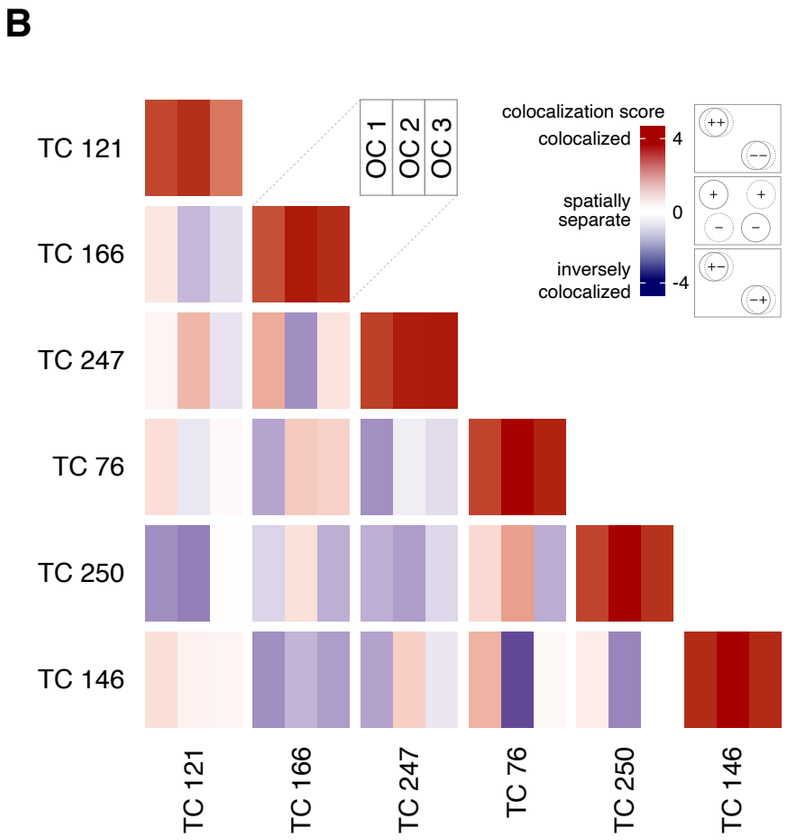
B
TC 121
TC 166
TC 247
TC 76
TC 250
TC 146
OC 1
OC 2
OC 3
colocalization score
colocalized
spatially separate
inversely colocalized
4
0
-4
++
−−
+
−
+−
−+

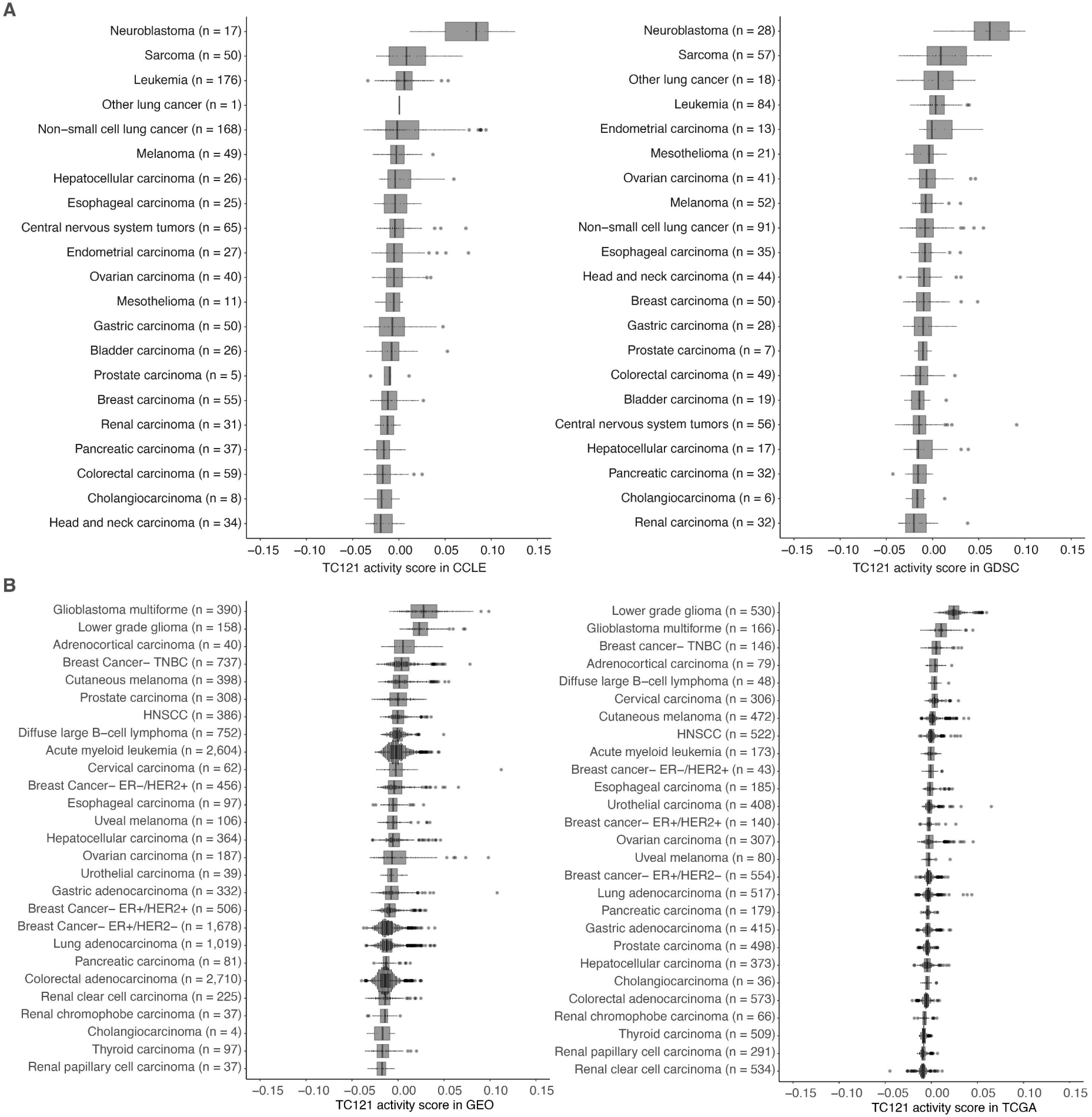
A
Neuroblastoma (n = 17)
Sarcoma (n = 50)
Leukemia (n = 176)
Other lung cancer (n = 1)
Non−small cell lung cancer (n = 168)
Melanoma (n = 49)
Hepatocellular carcinoma (n = 26)
Esophageal carcinoma (n = 25)
Central nervous system tumors (n = 65)
Endometrial carcinoma (n = 27)
Ovarian carcinoma (n = 40)
Mesothelioma (n = 11)
Gastric carcinoma (n = 50)
Bladder carcinoma (n = 26)
Prostate carcinoma (n = 5)
Breast carcinoma (n = 55)
Renal carcinoma (n = 31)
Pancreatic carcinoma (n = 37)
Colorectal carcinoma (n = 59)
Cholangiocarcinoma (n = 8)
Head and neck carcinoma (n = 34)
−0.15 −0.10 −0.05 0.00 0.05 0.10 0.15
TC121 activity score in CCLE
Neuroblastoma (n = 28)
Sarcoma (n = 57)
Other lung cancer (n = 18)
Leukemia (n = 84)
Endometrial carcinoma (n = 13)
Mesothelioma (n = 21)
Ovarian carcinoma (n = 41)
Melanoma (n = 52)
Non−small cell lung cancer (n = 91)
Esophageal carcinoma (n = 35)
Head and neck carcinoma (n = 44)
Breast carcinoma (n = 50)
Gastric carcinoma (n = 28)
Prostate carcinoma (n = 7)
Colorectal carcinoma (n = 49)
Bladder carcinoma (n = 19)
Central nervous system tumors (n = 56)
Hepatocellular carcinoma (n = 17)
Pancreatic carcinoma (n = 32)
Cholangiocarcinoma (n = 6)
Renal carcinoma (n = 32)
−0.15 −0.10 −0.05 0.00 0.05 0.10 0.15
TC121 activity score in GDSC
B
Glioblastoma multiforme (n = 390)
Lower grade glioma (n = 158)
Adrenocortical carcinoma (n = 40)
Breast Cancer− TNBC (n = 737)
Cutaneous melanoma (n = 398)
Prostate carcinoma (n = 308)
HNSCC (n = 386)
Diffuse large B−cell lymphoma (n = 752)
Acute myeloid leukemia (n = 2,604)
Cervical carcinoma (n = 62)
Breast Cancer− ER−/HER2+ (n = 456)
Esophageal carcinoma (n = 97)
Uveal melanoma (n = 106)
Hepatocellular carcinoma (n = 364)
Ovarian carcinoma (n = 187)
Urothelial carcinoma (n = 39)
Gastric adenocarcinoma (n = 332)
Breast Cancer− ER+/HER2+ (n = 506)
Breast Cancer− ER+/HER2− (n = 1,678)
Lung adenocarcinoma (n = 1,019)
Pancreatic carcinoma (n = 81)
Colorectal adenocarcinoma (n = 2,710)
Renal clear cell carcinoma (n = 225)
Renal chromophobe carcinoma (n = 37)
Cholangiocarcinoma (n = 4)
Thyroid carcinoma (n = 97)
Renal papillary cell carcinoma (n = 37)
−0.15 −0.10 −0.05 0.00 0.05 0.10 0.15
TC121 activity score in GEO
Lower grade glioma (n = 530)
Glioblastoma multiforme (n = 166)
Breast cancer− TNBC (n = 146)
Adrenocortical carcinoma (n = 79)
Diffuse large B−cell lymphoma (n = 48)
Cervical carcinoma (n = 306)
Cutaneous melanoma (n = 472)
HNSCC (n = 522)
Acute myeloid leukemia (n = 173)
Breast cancer− ER−/HER2+ (n = 43)
Esophageal carcinoma (n = 185)
Urothelial carcinoma (n = 408)
Breast cancer− ER+/HER2+ (n = 140)
Ovarian carcinoma (n = 307)
Uveal melanoma (n = 80)
Breast cancer− ER+/HER2− (n = 554)
Lung adenocarcinoma (n = 517)
Pancreatic carcinoma (n = 179)
Gastric adenocarcinoma (n = 415)
Prostate carcinoma (n = 498)
Hepatocellular carcinoma (n = 373)
Cholangiocarcinoma (n = 36)
Colorectal adenocarcinoma (n = 573)
Renal chromophobe carcinoma (n = 66)
Thyroid carcinoma (n = 509)
Renal papillary cell carcinoma (n = 291)
Renal clear cell carcinoma (n = 534)
−0.15 −0.10 −0.05 0.00 0.05 0.10 0.15
TC121 activity score in TCGA